DOI: 10.19884/j.1672-5220.202405008

Tension Active Disturbance Rejection Control of Automatic Yarn Splicing Robots for Ring Spinning

WANG Lisu[1], CAI Yun[2], JI Cheng[2], WANG Junliang[1*]
1. Institute of Artificial Intelligence, Donghua University, Shanghai 201620, China
2. Wuxi No. 1 Cotton Mill Textile Group CO. LTD., Wuxi 214101, China

Abstract: Automatic splicing of interrupted yarns in ring spinning has always been a problem in the industry. Factors such as low yarn strengths and environmental influence on yarn tensions make it difficult to control the yarn tension during the robotic splicing process. The purpose of this research is to design active disturbance rejection control (ADRC) for a third-order nonlinear tension system subject to external disturbances. Firstly, a third-order extended state observer (ESO) is designed to achieve the suppression and the compensation of the internal modeling error and the external disturbances of the system. Secondly, the adaptive gain error feedback control and the filtering process are designed to reduce the influence of sensor noise on the disturbance observation. Finally, the tension control during the splicing process is simulated and experimented, and the experiments show that the method has good robustness in the tension tracking task under a dynamic environment, which verifies the effectiveness of the method.

Key words: yarn splicing robot; tension control; active disturbance rejection control (ADRC); extended state observer (ESO)
CLC number: TS11 **Document code**: A
Article ID: 1672-5220(2024)05-0505-08

Open Science Identity (OSID)

0 Introduction

Ring spinning is a common spinning method in the textile industry. It is characterized by high production efficiency and good product quality. The ring-spun yarns are widely used in clothing, medical, aerospace and other fields[1]. However, the yarn interruption rate is high during the process of drafting and twisting the roving into spun yarns, which seriously affects the production efficiency. Currently, it is difficult to meet the large-scale and all-weather spinning demand by relying on manual splicing. The yarn tension during the splicing process is obviously affected by the environment. The splicing success rate of existing spun yarn automatic splicing robots is low[2]. Therefore, it is difficult to complete robot splicing in a dynamic environment. The control of yarn tension during the process is the key to improving the success rate of automatic splicing.

The current robot automatic splicing technology mainly uses the method of spinning up spare yarns. The spare yarn is wound on the broken yarn bobbin, and under the traction of the robot, it passes through the collector ring, the balloon ring and the yarn guide hook, and feeds the roller to complete the splicing[3]. During the spare yarn splicing process, the yarn tension mainly comes from two aspects: one is the traction force of the robot on the yarn, and the other is the tension generated by the rewinding and unwinding of the spare bobbin. Since the movement of the manipulator during the splicing process is fixed and therefore cannot be changed, the control mainly relies on the control of the retraction and release of the spare bobbin. By controlling the retracting and the unwinding speed of the spare bobbin, effective yarn tension control can be achieved to ensure that the yarn tension during the splicing process is within an appropriate range. Due to the interference of internal uncertainties and external factors such as the characteristics of the yarn, environmental factors and the motion characteristics of the robot, the yarn tension will be disturbed. When the tension exceeds the breaking strength, the yarn will break and the splicing will fail. Many scholars have proposed various methods to suppress disturbances. Nonlinear robust control is a relatively mature method. The advantage of robustness is that it can remain stable in the face of a large number of disturbances[4-5]. In recent years, sliding mode variable structure control[6-7], feedforward compensation

Received date: 2024-05-15
Foundation items: National Natural Science Foundation of China (No. 52275478); Fundamental Research Funds for the Central Universities, China (No. 2232024Y-01); DHU Distinguished Young Professor Program, China (No. LZB2023001)
* Correspondence should be addressed to WANG Junliang, email: junliangwang@dhu.edu.cn
Citation: WANG L S, CAI Y, JI C, et al. Tension active disturbance rejection control of automatic yarn splicing robots for ring spinning[J]. *Journal of Donghua University (English Edition)*, 2024, 41(5): 505-512.

control[8-9], neural network control[10-12] and active disturbance rejection control (ADRC)[13] have been developed. Among them, ADRC has received widespread attention due to its high robustness and immunity to disturbance. Wei et al.[14] proposed a phase-advance ADRC to estimate the hysteresis and improve the positioning performance of the nanopositioning stage. An excellent work by Guo et al.[15] introduced ADRC from the theoretical perspective of nonlinear systems. Huang et al.[16] and Feng et al.[17] gave recent reviews of ADRC methods and theoretical analyses.

ADRC first uses an extended state observer (ESO) to reconstruct the system state and estimate the so-called total disturbance (including unmodeled dynamics and external disturbance). This estimate is then used to generate an inner loop compensation for the total disturbance. ESO achieves fast convergence and high accuracy through high gain. However, the high gain makes ESO sensitive to measurement noise which is amplified by ESO and added to ESO-based systems[18]. This can lead to adverse effects such as vibration of the mechanical system, saturation of the input actuators and even system instability. Therefore, the compensation performance is limited.

Several strategies have been proposed in the literature to overcome this limitation. ESO cascades were proposed to avoid over-amplification of measurement noise by decomposing the total disturbance into multiple parts within a predefined frequency range and using different gains for the cascade observer[19-20]. Du et al.[21] designed a new ESO structure that separated the estimate of the total disturbance from the reconstruction of the system state, and used new parameters to adjust the disturbance estimate instead of the bandwidth of the observer, making the observer's gain relatively low. Khalil et al.[22] designed a gain adjustment method to reduce the impact of measurement noise by adopting a high gain during the transient response and a low gain during the steady state. Composite observers combining ESO with Kalman filters improved the disturbance estimate of systems with uncertainties and zero-mean Gaussian white measurement noise[23-25]. Although these methods have shown effectiveness in reducing the impact of measurement noise on disturbance estimates, they increase the complexity of the system design. Thus adjusting the ESO gain seems to be an effective method to overcome noise sensitivity.

Therefore, the tension in the automatic splicing process of ring-spun yarns is taken as the research object, and a mathematical model of the tension servo system is established based on the dynamic characteristics of its working process. The adaptive gain state estimation strategy is used to avoid noise amplification. By designing an active disturbance rejection controller, a tension active disturbance rejection model is established. The system is simulated and tested.

1 Control Design

1.1 Tension active disturbance rejection control system

The schematic diagram of the ring spinning automatic splicing tension control mechanism is shown in Fig. 1. The servo motor directly drives the yarn tube to rotate. The tension is converted into an angle signal through the combination of the tension rod and the tension spring. At the same time, the tension spring buffers the yarn and prevents breaking of the yarn. The angle sensor is connected to the embedded micro control unit (MCU), which can realize real-time feedback adjustment of tension.

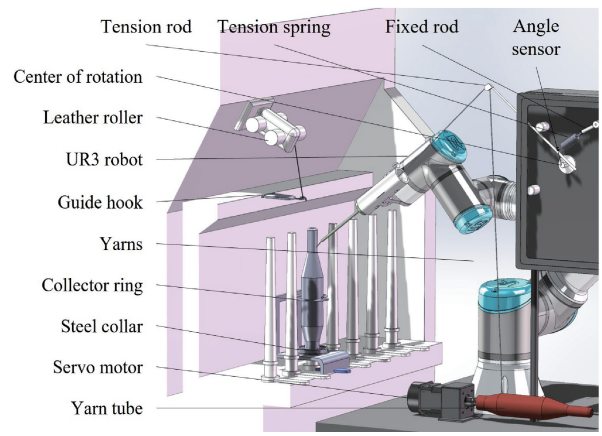

Fig. 1 Schematic diagram of ring spinning automatic splicing tension control

Tension control mainly includes the following parts:

1) After powering on, the host computer issues reference instructions to the MCU.

2) The MCU realizes the rewinding and unwinding of the spare bobbin through driving the servo motor.

3) The signal of the angle sensor is sent to the embedded chip through the analog-to-digital converter (ADC). The sensor signal is fed back to the data acquisition module of the controller in real time. The data acquisition module adjusts the parameters appropriately through the tension auto-disturbance rejection closed-loop control algorithm and then feeds it back to drive the servo motor. Figure 2 shows the model of the whole control system which consists of a step signal input, the tracking differentiator (TD) filtering of the input signal, the adaptive gain error feedback control (EFC), the plant and the ESO.

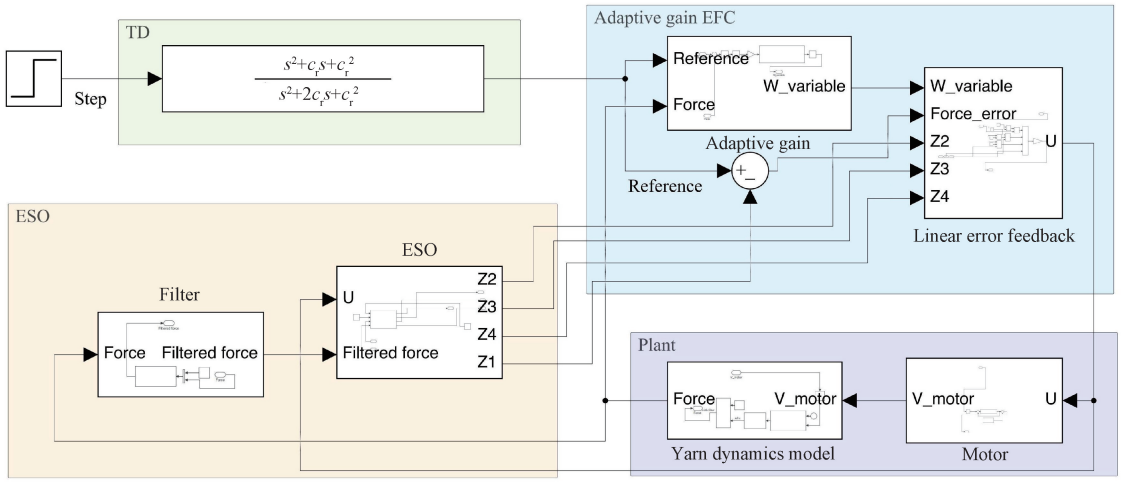

s—complex variable in Laplace transform; c_r—bandwidth of TD; W_variable—bandwidth of ADRC calculated from actual force and reference force; force_error—difference between actual force and reference force; V_motor—actual speed of motor; U—output of linear error feedback.

Fig. 2 Control system structure diagram

1.2 Yarn force model

The force model of the yarn is shown in Fig. 3. The tension rod amplifies the force through leverage. The tension spring converts the force into the angular displacement of the angle sensor.

The yarn force T can be obtained from the lever principle and Hooke's law:

$$T=\frac{kR_0R_2\sin(\theta+\theta_0)}{R_1}\left\{1-\frac{R_3+L_0}{\sqrt{[R_2\sin(\theta+\theta_0)]^2+[R_2\cos(\theta+\theta_0)-R_0]^2}}\right\}, \tag{1}$$

where R_1 is the length of the tension rod; θ is the angle of the tension rod; R_3 is the length of the fixed rod; R_2 is the distance from the fixed rod to the rotation center; θ_0 is the angle of the fixed rod; k is the Hooke coefficient of the spring; L_0 is the original length of the tension spring; R_0 is the distance from the fixed point of the spring to the rotation center.

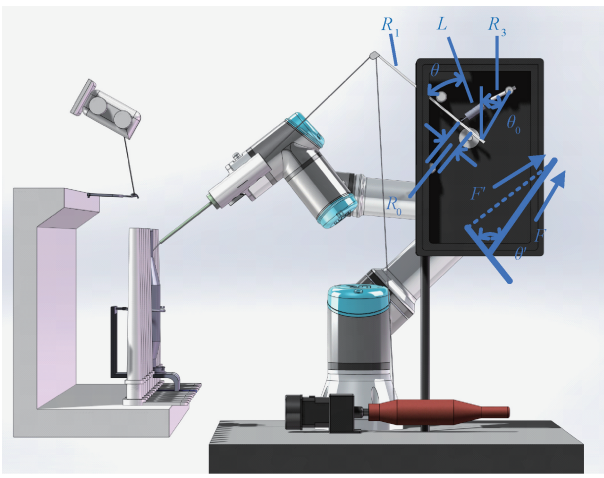

Fig. 3 Yarn force model

1.3 Yarn dynamics model

Taking the movement of the yarn as the research object, the dynamic equations can be obtained from the geometric equation:

$$\int\frac{\mathrm{d}(v_{\text{motor}}-v_{\text{env}})}{\mathrm{d}t}=\sqrt{(R_1\sin\theta_1-x_1)^2+(R_1\cos\theta_1-y_1)^2}+\sqrt{(R_1\sin\theta_1-x_2)^2+(R_1\cos\theta_1-y_2)^2}-\sqrt{(R_1\sin\theta_2-x_1)^2+(R_1\cos\theta_2-y_1)^2}-\sqrt{(R_1\sin\theta_2-x_2)^2+(R_1\cos\theta_2-y_2)^2}, \tag{2}$$

where θ_1 and θ_2 are tension rod angles; (x_1, y_1) and (x_2, y_2) are line loop positions; v_{motor} is the servo motor speed; v_{env} is the external environment speed acting on the yarn.

The dynamic model of the servo motor is obtained through identification, and the fitted transfer function $G_{\text{m}}(s)$ is

$$G_{\text{m}}(s)=\frac{p_4}{p_1s^2+p_2s+p_3}, \tag{3}$$

where p_1, p_2, p_3 and p_4 are the identified parameters.

1.4 Tension active disturbance rejection controller

The tension active disturbance rejection controller consists of two parts: an ADRC controller and an adaptive gain ESO controller.

1.4.1 ADRC controller

In order to obtain good transient control performance, the differential tracker is formed by a stable linear filter:

$$\begin{aligned}\dot{\boldsymbol{x}}&=\begin{bmatrix}0&1\\c_r^2&-2c_r\end{bmatrix}\boldsymbol{x}+\begin{bmatrix}0\\1\end{bmatrix}\boldsymbol{u},\\ \boldsymbol{y}&=\begin{bmatrix}c_r^2&0\end{bmatrix}\boldsymbol{x}+\boldsymbol{u},\end{aligned} \tag{4}$$

where $\boldsymbol{y}$ is the output; $\boldsymbol{x}$ is the state of the system; $\boldsymbol{u}$ is the controlled variable.

Consider a class of control systems affected by uncertainties:

$$\begin{cases}\dot{\boldsymbol{x}}(t) = \boldsymbol{A}\boldsymbol{x}(t) + \boldsymbol{B}[b(\boldsymbol{x}(t), t)\boldsymbol{u}(t) + \\ \qquad f(\boldsymbol{x}(t)) + \boldsymbol{d}(t)], \\ \boldsymbol{y}(t) = \boldsymbol{C}\boldsymbol{x}(t), \end{cases} \tag{5}$$

where

$$\boldsymbol{A} = \begin{bmatrix} 0 & 1 & 0 & \cdots & 0 \\ 0 & 0 & 1 & \cdots & 0 \\ \vdots & \vdots & \vdots & & \vdots \\ 0 & 0 & 0 & \cdots & 1 \\ 0 & 0 & 0 & \cdots & 0 \end{bmatrix}; \boldsymbol{B} = \begin{bmatrix} 0 \\ 0 \\ \vdots \\ 0 \\ 1 \end{bmatrix}; \boldsymbol{C} = \begin{bmatrix} 1 \\ 0 \\ \vdots \\ 0 \\ 0 \end{bmatrix}^{\mathrm{T}};$$

$\boldsymbol{x}(t) = [x_1(t), x_2(t), \cdots, x_n(t)]^{\mathrm{T}} \in \mathbf{R}^n$ is the system state; $f: \mathbf{R}^n \to \mathbf{R}$ is the unknown nonlinear dynamics; $\boldsymbol{d} \in \mathbf{R}^n$ is the external disturbance, and $d_i \geqslant 0 (i = 1, 2, \cdots, n)$; $b: \mathbf{R}^n \times \mathbf{R} \to \mathbf{R}$ is the unknown control input gain function; $\boldsymbol{u} \in \mathbf{R}^n$ is the control input; $\boldsymbol{y} \in \mathbf{R}^n$ is the measurement output.

Obviously, if $\boldsymbol{x}(t)$, $f(\boldsymbol{x}(t))$, $\boldsymbol{d}(t)$ and $b(\boldsymbol{x}(t), t)$ are known, $\boldsymbol{u}^*(t)$ will make the actual trajectory $\boldsymbol{x}(t)$ converge to the reference signal $\boldsymbol{r}(t)$:

$$\boldsymbol{u}^*(t) = \frac{-\boldsymbol{K}^{\mathrm{T}}(\boldsymbol{x}(t) - \boldsymbol{r}(t) - \boldsymbol{f}(\boldsymbol{x}(t)) - \boldsymbol{d}(t))}{b(\boldsymbol{x}(t), t)}, \tag{6}$$

where $\boldsymbol{K} = [k_1, k_2, \cdots, k_n]$.

However, the measurement output only gives $x_1(t)$. In addition, it is almost impossible to obtain the real value of $f(\boldsymbol{x}(t))$, $\boldsymbol{d}(t)$ and $b(\boldsymbol{x}(t), t)$. Despite these difficulties, it is possible to estimate $\boldsymbol{x}(t)$ and the uncertainties in real time by designing the ESO and applying the ADRC law to adjust the closed-loop performance while eliminating the effects of the uncertainties. Therefore, due to its simple structure and easy adjustment, the following linear ESO (LESO) is designed to accomplish this task:

$$\begin{cases}\dot{\hat{x}}_i(t) = \hat{x}_i(t) + \beta_i(x_1(t) - \hat{x}_1(t)), \\ \qquad i = 1, 2, \cdots, n-1, \\ \dot{\hat{x}}_n(t) = \hat{x}_{n+1}(t) + b_0(t)u(t) + \beta_n(x_1(t) - \hat{x}_1(t)), \\ \dot{\hat{x}}_{n+1}(t) = \beta_{n+1}(x_1(t) - \hat{x}_1(t)), \end{cases} \tag{7}$$

where $b_0(t)$ is the standard value of $b(\boldsymbol{x}(t), t)$ and can be obtained through experimental data modeling or online identification algorithm; $\hat{\boldsymbol{x}}_i(t)$ is the estimate of $\boldsymbol{x}_i(t)$; $\hat{x}_{n+1}(t)$ is the total disturbance estimate of $x_{n+1}(t)$; $\boldsymbol{\beta} = [\beta_1, \beta_2, \cdots, \beta_{n+1}]^{\mathrm{T}}$ is the observer gain, and satisfies

$$(s + \omega_o)^{n+1} = s^{n+1} + \beta_1 s^n + \beta_2 s^{n-1} + \cdots + \beta_{n+1}, \tag{8}$$

with the bandwidth ω_o being adjusted ($\omega_o > 0$).

After designing LESO, the ADRC control rate can be designed as

$$u(t) = \frac{-\sum_{i=1}^{n} k_i(\hat{x}_i(t) - r_i(t)) - \hat{x}_{n+1} + r_{n+1}(t)}{b_0(t)}. \tag{9}$$

In order to track the reference signal $\boldsymbol{r}(t)$ by $x_1(t)$, $r_i = r^{(i-1)}$, $k_i > 0$, $i = 1, 2, \cdots, n$. The whole system can be seen in Fig. 4. Assuming $\boldsymbol{e}(t) = \boldsymbol{x}(t) - \boldsymbol{r}(t)$, $\hat{\boldsymbol{e}}(t) = [\boldsymbol{x}^{\mathrm{T}}(t) - \hat{\boldsymbol{x}}^{\mathrm{T}}(t), x_{n+1}(t) - \hat{x}_{n+1}(t)]^{\mathrm{T}}$, the tracking error of the system can be equivalently expressed:

$$\dot{\boldsymbol{e}}(t) = \boldsymbol{A}_1\boldsymbol{e}(t) + \boldsymbol{B}\bar{\boldsymbol{K}}\hat{\boldsymbol{e}}(t), \tag{10}$$

where $\boldsymbol{A}_1 = \boldsymbol{A} - \boldsymbol{B}_1\boldsymbol{K}$; $\bar{\boldsymbol{K}} = [k_1, k_2, \cdots, k_n, 1]$.

Because $\boldsymbol{A}_1$ is a Hurwitz matrix, the system has input-to-state stability (ISS), that is, there are Kullback-Leibler ($\mathcal{KL}$)-class functions α_e and $\mathcal{K}$-class functions γ_e such that

$$\|\boldsymbol{e}(t)\| \leqslant \alpha_e(\|\boldsymbol{e}(t_0)\|, t - t_0) + \gamma_e(\sup_{\tau \in [0,t)} \|\hat{\boldsymbol{e}}(\tau)\|), \tag{11}$$

where t_0 represents the initial time. Obviously, if the estimate error of ESO is bounded, then the closed-loop system is also bounded.

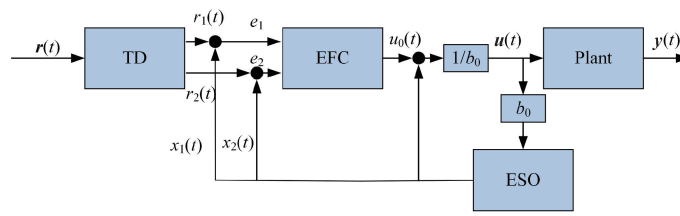

Fig. 4 Classic ADRC control block diagram

1.4.2 Adaptive gain ESO controller

High-order ESO will be affected by sensor noise. High-frequency sensor noise will cause the system to oscillate. Generally speaking, a low-pass filter (LPF) is a common method to solve sensor noise. A traditional second-order LPF is designed, and its state space equation is

$$\begin{cases}\dot{\boldsymbol{g}} = \begin{bmatrix} 0 & 1 \\ -w_0^2 & -2w_0 \end{bmatrix}\boldsymbol{g} + \begin{bmatrix} 0 \\ 1 \end{bmatrix}\boldsymbol{u}, \\ y_1(\boldsymbol{y}(t)) = [w_0^2 \quad 0]\boldsymbol{g} + \boldsymbol{u}, \end{cases} \tag{12}$$

where w_0 is the filter cut-off frequency; g is intermediate state. We combine ESO with LPF:

$$\begin{cases}\dot{\hat{x}}_i(t) = \hat{x}_i(t) + \beta_i g_1(t), \quad i = 1, 2, \cdots, n-1, \\ \dot{\hat{x}}_n(t) = \hat{x}_{n+1}(t) + b_0(t)u(t) + \beta_n g_1(t), \\ \dot{\hat{x}}_{n+1}(t) = \beta_{n+1} g_1(t), \\ \dot{\boldsymbol{g}}_f(t) = \begin{bmatrix} 0 & 1 \\ -w_0^2 & -2w_0 \end{bmatrix}\boldsymbol{g}_f(t) + (\boldsymbol{x}_1(t) - \hat{\boldsymbol{x}}_1(t)). \end{cases} \tag{13}$$

In this section, the following new error-driven adaptive-gain error feedback control (EFC) is proposed to provide the control signal:

$$\begin{cases} u = -\dfrac{1}{b_0}\left[a_1(\hat{x}_1 - r) + a_2\hat{x}_2 + a_3\hat{x}_3 + \hat{x}_4\right], \\ a_i = C_n^{n+1-i}\omega_x^{\,n+1-i}(i = 1,2,3), \\ e = g_a \times |r(t) - y(t)|, \\ \dot{z} = \begin{bmatrix} 0 & 1 \\ -c_r^{\,2} & -2c_r \end{bmatrix} z + \begin{bmatrix} 0 \\ 1 \end{bmatrix} e, \\ \omega_y = [0 \quad -c_r]\, z + u, \\ \omega_x = \begin{cases} u_{pp}, & \text{if } \omega_{y1} > u_{pp}, \\ \omega_{y1}, & \text{if } u_{pp} \leqslant \omega_{y1} \leqslant l_{ow}, \\ l_{ow}, & \text{if } \omega_{y1} < l_{ow}. \end{cases} \end{cases} \tag{14}$$

where g_a is the variable gain; u_{pp} is the upper limit of the bandwidth; l_{ow} is the lower limit of the bandwidth; z is intermediate state.

2 Results and Discussion

In order to verify the feasibility and the effectiveness of the proposed controller, a simulation and an experiment on the force tracking control scenario of the piecing robot for ring spinning were conducted. The hyperparameters are shown in Table 1.

Table 1 Hyperparameter table for system simulation

Hyperparameter	Value	Hyperparameter	Value
R_0	0.013 5	c_r	100
R_1	0.215 0	w_c	200
R_2	0.093 9	w_0	600
R_3	0	b_0	360 000
k	105	g_a	1 600
L_0	0.050 0	u_{pp}	200
q_1	$-5\pi/18$	l_{ow}	120

2.1 Simulation results and analyses

The expected tension is 4.0 cN, the operating cycle is 2.000 s, and an external disturbance of 2 m/s starts at 1.000 s and is cancelled at 1.500 s.

Figure 5 shows the simulation results of the step responses of the five controllers. The PID controller has been optimized by particle swarm optimization (PSO-PID). The adaptive gain controller is the designed controller. The ADRC is the traditional controller with LESO. The improved-ESO (IESO) controller has a high-order observer[26]. The variable band controller is the ADRC controller with the variable band controller[27]. The maximum deviation of the adaptive gain controller is 6.40%, and is 0.37% less than that of the PSO-PID controller. The tuning time of the adaptive gain controller is 0.115 s, which is lower than that of variable band, ADRC and IESO controllers.

In order to demonstrate the anti-interference performance, an external disturbance with a speed of 1 m/s acting on the yarn was added at 1.000 s, and the disturbance was removed at 1.500 s. The simulation results are shown in Fig. 6. The response time of the adaptive gain controller is 0.016 s, it is 0.021 s less than that of the ADRC controller. The maximum deviation of the adaptive gain controller is 28.95%, which is close to the performance of the optimal disturbance suppression algorithm variable band, 21.25%.

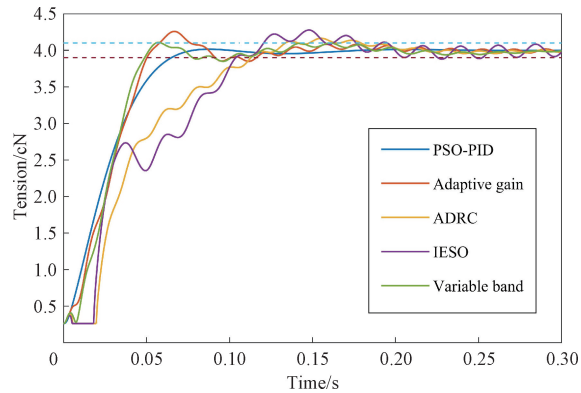

Fig. 5 Step response curve

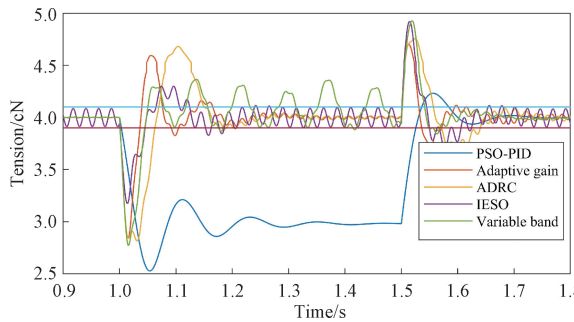

Fig. 6 Interference response curve

Due to the influence of modeling and internal parameters, internal disturbances are generated. Figure 7 simulates the response curve after adding internal disturbances. The variable band controller and the IESO controller have weak performance in suppressing internal disturbances, and the adaptive gain controller has similar performance to the ADRC controller.

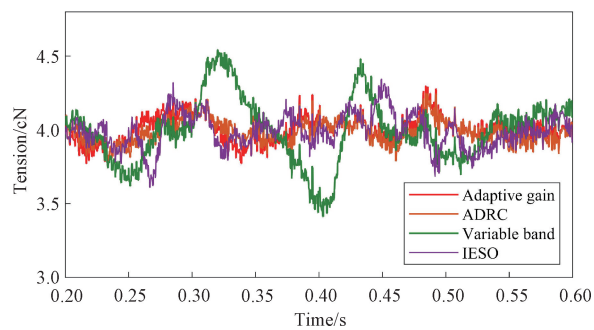

Fig. 7 Internal disturbance response curve

Sensor noise is suppressed by adjusting the gain and adding noise filtering. Thus the noise influence of disturbance estimate can be reduced. Figure 8 simulates the system response curve with a noise power of 0.000 001 and a sampling time of 0.000 5 s. The steady-

state response of the adaptive gain controller has less fluctuation than the ADRC controller and the variable band controller.

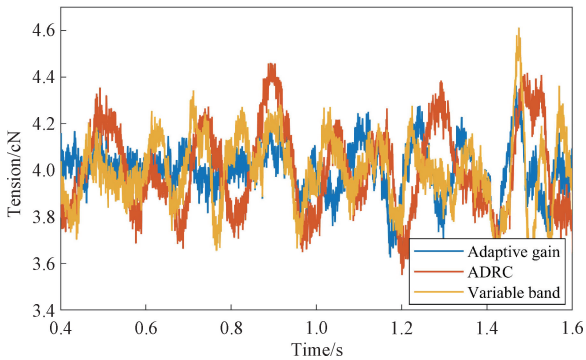

Fig. 8 System response curve under sensor noise

2.2 Experimental results and analyses

The experiment is carried out on the ring spinning automatic splicing robot platform, as shown in Fig. 9. The experimental flow is shown in the control system in Fig. 2. One end of the MCU STM32F407IGT6 is connected to the servo driver, driving the servo motor through space vector pulse width modulation (SVPWM), and the other end is connected to the angle sensor as a force feedback. The tension sensor FS1-200 is connected as an objective tension observation which is connected to the computer. The data is analyzed on the computer.

Based on the above design, tension active disturbance rejection control is applied in two operating conditions in the ring spinning splicing process. In addition, PSO-PID and IESO controllers are designed as control groups. Figure 10 shows the tension curves at the two working cases in the ring spinning splicing process, and the working tension is 2 cN. Figure 10(a) shows the step response of controllers and Fig. 10(b) shows the yarn pulling response of controllers. The step response time of the adaptive gain controller is 0.074 s, and the step response time of the IESO controller is close to that of the ADRC controller at 0.062 s, and the maximum deviation amounts of the three are close to each other, and the performance of the step response is similar. The response time of the adaptive gain controller under external disturbance is 0.057 s, which is 5% shorter than the response time of IESO and ADRC controllers, and the adaptive gain controller responds faster and can return to the steady state faster.

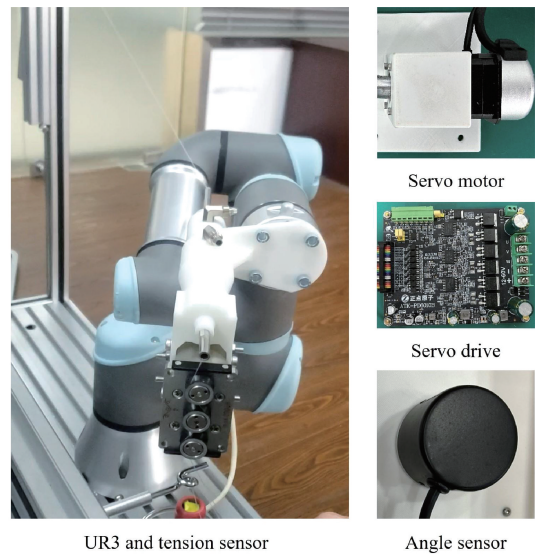

Fig. 9 Ring spinning automatic splicing robot platform

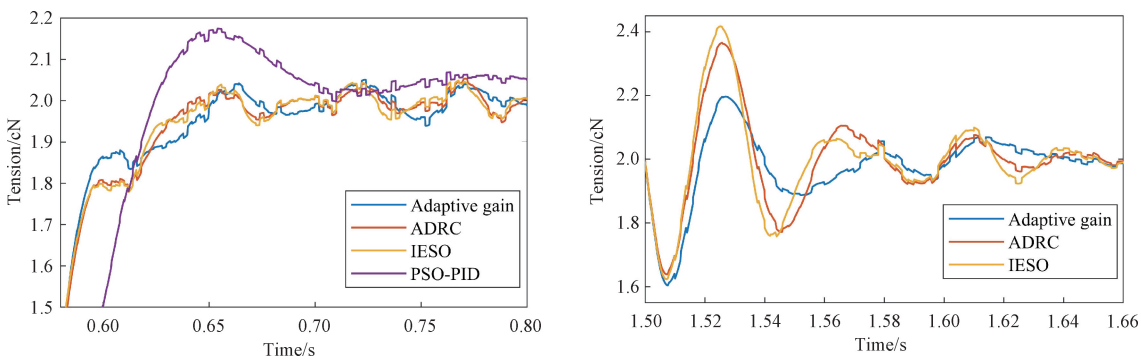

Fig. 10 Tension curves in ring spinning automatic splicing process: (a) step response; (b) yarn pulling response

The steady-state tension fluctuations are shown in Fig. 11. The tension variance of the adaptive gain controller in the steady state is 0.017 2 cN^2, while that of the ADRC controller and the IESO controller is 0.019 4 and 0.020 6 cN^2, respectively. The tension variance of the PSO-PID controller is the smallest. Thus the adaptive gain controller has a good performance in terms of noise suppression.

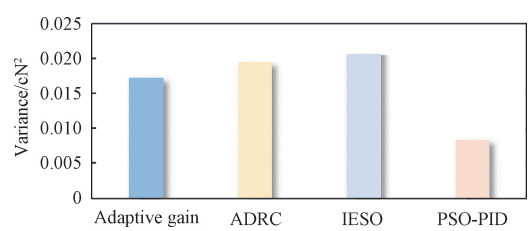

Fig. 11 Steady-state tension fluctuations

3 Conclusions

In this paper, a tension control strategy based on a self-immobilizing controller is proposed for the problem of tension control of the ring spinning splicing robot, and a force tracking model is designed. An ESO is designed to suppress internal and external disturbances, and a second-order Butterworth filter is used to filter out the high-frequency signal of the sensor. The adaptive gain controller is used to overcome the high gain generated by the ESO that is sensitive to sensor noise. The simulation results show that the maximum deviation of the proposed adaptive gain controller is 6.40%, and the disturbance response time is 0.017 s. The experiment shows that the proposed control method has a strong immunity to interference, a high convergence speed and a maximum deviation suppression ability, and it would be used in tension control of the yarn splicing robot. How to adaptively optimize the control gain to achieve the stability of force tracking and the convergence of the controller will be studied.

References

[1] PENG Z Y, LI W, XU D, et al. Analysis of ring spinning technology and construction of ideal yarn structure[J]. *Cotton Textile Technology*, 2023, 51(11): 1-6. (in Chinese)

[2] TANG X J, SONG J Y, HE X D. Technology progress of ring spinning automatic piecing device at home and abroad [J]. *Cotton Spinning Technology*, 2019, 47(1): 78-84. (in Chinese)

[3] ZHANG Y S, WANG X H, HE Y. Research progress on key technology of ring spinning frame automatic joint[J]. *Cotton Textile Technology*, 2023, 51(10): 90-96. (in Chinese)

[4] KOLHE J P, SHAHEED M, CHANDAR T S, et al. Robust control of robot manipulators based on uncertainty and disturbance estimation [J]. *International Journal of Robust and Nonlinear Control*, 2013, 23(1): 104-122.

[5] ISLAM S, LIU P X, EL SADDIK A. Robust control of four-rotor unmanned aerial vehicle with disturbance uncertainty [J]. *IEEE Transactions on Industrial Electronics*, 2015, 62(3): 1563-1571.

[6] RIAZ M, YASIN A R, ARSHAD UPPAL A, et al. A novel dynamic integral sliding mode control for power electronic converters [J]. *Science Progress*, 2021, 104 (4): 003685042110448.

[7] QU Y, ZHANG B, CHU H R, et al. Sliding-mode anti-disturbance speed control of permanent magnet synchronous motor based on an advanced reaching law[J]. *ISA Transactions*, 2023, 139: 436-447.

[8] HOU Q K, DING S H, YU X H. Composite super-twisting sliding mode control design for PMSM speed regulation problem based on a novel disturbance observer[J]. *IEEE Transactions on Energy Conversion*, 2021, 36(4): 2591-2599.

[9] NAWRESS B, LAKHAL A N G, BRAÏEK N B. Neural state and disturbance observer-based sliding mode control of a unicycle robot[C]// 2023 IEEE International Conference on Advanced Systems and Emergent Technologies. Hammamet, Tunisia: IEEE, 2023: 1-6.

[10] YANG G C, YAO J Y, DONG Z L. Neuroadaptive learning algorithm for constrained nonlinear systems with disturbance rejection[J]. *International Journal of Robust and Nonlinear Control*, 2022, 32(10): 6127-6147.

[11] HE T F, WU Z. Neural network disturbance observer with extended weight matrix for spacecraft disturbance attenuation[J]. *Aerospace Science and Technology*, 2022, 126: 107572.

[12] CHENG X, LU W K, LIU H S. Adaptive neural network control for Euler-Lagrangian systems with uncertainties [J]. *Journal of Donghua University (English Edition)*, 2022, 39(5): 485-489.

[13] HAN J Q. From PID to active disturbance rejection control [J]. *IEEE Transactions on Industrial Electronics*, 2009, 56(3): 900-906.

[14] WEI W, ZHANG Z Y, ZUO M. Phase leading active disturbance rejection control for a nanopositioning stage [J]. *ISA Transactions*, 2021, 116: 218-231.

[15] GUO B Z, ZHAO Z L. Active disturbance rejection control for nonlinear systems: an introduction [M]. Hoboken, NJ, USA: John Wiley & Sons, 2017.

[16] HUANG Y, XUE W C. Active disturbance rejection control: methodology and theoretical analysis[J]. *ISA Transactions*, 2014, 53(4): 963-976.

[17] FENG H, GUO B Z. Active disturbance rejection control: old and new results[J]. *Annual Reviews in Control*, 2017, 44: 238-248.

[18] SARIYILDIZ E, OBOE R, OHNISHI K. Disturbance observer-based robust control and its applications: 35th anniversary overview [J]. *IEEE Transactions on Industrial Electronics*, 2020, 67(3): 2042-2053.

[19] ŁAKOMY K, MADONSKI R. Cascade extended state observer for active disturbance rejection control applications under measurement noise [J]. *ISA Transactions*, 2021, 109: 1-10.

[20] LAKOMY K, MADONSKI R, DAI B, et al. Active disturbance rejection control design with suppression of sensor noise effects in application to DC-DC buck power converter [J]. *IEEE Transactions on Industrial Electronics*, 2022, 69

(1): 816-824.
[21] DU Y W, CAO W H, SHE J H. Analysis and design of active disturbance rejection control with an improved extended state observer for systems with measurement noise [J]. *IEEE Transactions on Industrial Electronics*, 2023, 70(1): 855-865.
[22] KHALIL H K, PRIESS S. Analysis of the use of low-pass filters with high-gain observers [J]. *IFAC-PapersOnLine*, 2016, 49(18): 488-492.
[23] BAI W Y, XUE W C, HUANG Y, et al. On extended state based Kalman filter design for a class of nonlinear time-varying uncertain systems [J]. *Science China Information Sciences*, 2018, 61(4): 042201.
[24] SUN H, MADONSKI R, LI S H, et al. Composite control design for systems with uncertainties and noise using combined extended state observer and Kalman filter [J]. *IEEE Transactions on Industrial Electronics*, 2022, 69(4): 4119-4128.
[25] XUE W C, BAI W Y, YANG S, et al. ADRC with adaptive extended state observer and its application to air-fuel ratio control in gasoline engines [J]. *IEEE Transactions on Industrial Electronics*, 2015, 62(9): 5847-5857.
[26] HOU Q, ZUO Y, WANG H, et al. High-order NESO based enhanced ADRC for PMSM drives considering uncertainty and measurement noise suppression [C]//IECON 2022-48th Annual Conference of the IEEE Industrial Electronics Society. New York: IEEE, 2022: 1-6.
[27] ZHANG J, CUI C, GU S, et al. Trajectory tracking control of pneumatic servo system: a variable gain ADRC approach [J]. *IEEE Transactions on Cybernetics*, 2022, 53(11): 6977-6986.

环锭纺细纱自动接头机器人张力自抗扰控制

王立甦[1], 蔡 赟[2], 季 承[2], 汪俊亮[1*]
1. 东华大学 人工智能研究院, 上海 201620
2. 无锡一棉纺织集团, 江苏 无锡 214101

摘 要: 环锭纺工艺中断纱的自动接头一直是行业难题。纱线强度低、纱线张力受环境因素影响等因素使得机器人接头过程中的纱线张力难以控制。该文旨在解决受外部干扰的三阶非线性张力系统的自抗扰控制问题。首先, 设计了三阶扩张状态观测器, 以实现对系统内部建模误差和外部干扰的抑制和补偿; 其次, 设计了可变增益误差反馈控制率和滤波过程减少传感器噪声对扰动观测的影响; 最后, 对接头过程中的纱线张力进行模拟和试验验证。试验表明, 该方法在动态环境下的张力跟踪任务中具有良好的鲁棒性, 该方法的有效性得到验证。

关键词: 细纱接头机器人; 张力控制; 自抗扰控制; 扩张状态观测器